Interface and longitudinal optical phonon modes in cylindrical quantum dots

Clément Kanyinda-Malu* and Rosa María de la Cruz†
Departamento de Física, Universidad Carlos III de Madrid, c/Butarque 15, 28911 Leganés, (Madrid) Spain
(Received 29 April 1998; revised manuscript received 28 August 1998)

We report the interface and longitudinal-optical phonon modes in cylindrical quantum dots using the dielectric-continuum model. We also investigate the effect of the dot surrounding materials on both the top-surface optical (TSO) and the side-surface optical (SSO) phonon modes. We observe that the symmetric and antisymmetric TSO modes are cylinder-radius dependent for the heterostructure system. On the other hand, in the free-standing dots, only the symmetric TSO branch shows a significant dependence with the cylinder radius, while the SSO modes are cylinder-radius independent for the large radius in both cases. [S0163-1829(99)00603-7]

I. INTRODUCTION

Recent advances in nanostructural techniques, like molecular-beam epitaxy and metal-organic chemical-vapor deposition, have made it possible to produce semiconductor quantum wires and dots with spherical, cylindrical, and rectangular shapes of an optimal quality.[1] It has been found that quantum dots are self-assembled into pyramidal shapes because of the competition between the surface and interface tensions. Atomic force microscopy observations reveal that islands of InAs are spontaneously formed when an InAs layer with thickness above 1.7 ML is deposited by MBE on the GaAs {100} planes.[2,3]

Due to the claims of the lasing effect and their potential applications in microelectronic devices, theoretical and experimental studies are intensively devoted to these artificially structured materials. An electron in a polar semiconductor interacts with the interface and bulk longitudinal-optical (LO) phonons. This interaction can produce the localization of the electron near the interface,[1,4] changing its effective mass.

The electron-phonon interactions have been investigated in quantum wires and dots with different geometrical shapes.[5–7] Recently, Li and Chen have calculated the confined LO and surface-optical (SO) phonon modes for cylindrical free-standing dots.[8] They have found modes associated with the top-surface optical (TSO) and the side-surface optical (SSO) phonons of the quantum dot obtaining their electron-phonon Fröhlich Hamiltonians.

Although there exists a large amount of work about the electron-IF phonon interactions,[1–9,11–13] few papers concern surface phonon frequencies in cylindrical quantum dots. Interface frequencies are needed to obtain the Fröhlich coupling constants giving the strength of electron-phonon interaction in semiconductors. In this paper, following the model of Li and Chen,[8] we calculate the SO phonon modes as a function of the confinement for cylindrical quantum dots. First, we study the free-standing systems in a vacuum, then we extend the calculations for GaAs/AlAs and InAs/GaAs quantum dots. Throughout this paper, we refer to SO modes to describe both the surface and interface modes in free-standing and heterostructure systems, respectively.

II. THEORETICAL FORMALISM

We consider the heterostructure formed by a cylindrical polar semiconductor 1 of radius R and height $2d$ embedded in another polar semiconductor 2, both characterized by their wave-vector-independent lattice dielectric functions $\epsilon_1(\omega)$ and $\epsilon_2(\omega)$. For the free-standing system $\epsilon_2=1$ and, then the polarization outside the dot material is identically null.

The dielectric continuum approximation predicts the existence of SO modes that differ from the LO phonons at the quantum-dot surface.[9] In this approach, the electron-phonon interaction is obtained from the electrostatic potential taking into account the polarization of the material. In the absence of free charges in the dot and in the barrier material, and using Maxwell equations, the electrostatic potential must satisfy $\epsilon(\omega)\nabla^2\Phi(\mathbf{r})=0$ where ϵ is the dielectric function and $\Phi(\mathbf{r})$ represents the electrostatic potential. Solutions to this equation inside the quantum dot can be obtained imposing $\epsilon(\omega)=0$. This yields the bulk LO mode whose frequency is ω_{LO}. The remaining solutions are found from Laplace's equation $\nabla^2\Phi(\mathbf{r})=0$.

In each polar semiconductor, the frequency-dependent dielectric function is expressed by the Lyddane-Sachs-Teller relation as

$$\epsilon_i(\omega)=\epsilon_{i,\infty}+\frac{(\epsilon_{i,0}-\epsilon_{i,\infty})}{1-\omega^2/\omega_{i,TO}^2} \quad (i=1,2), \tag{1}$$

where $\epsilon_{i,0}$ and $\epsilon_{i,\infty}$ are the static and high-frequency dielectric constants, respectively, and $\omega_{i,TO}$ is the frequency of the transverse-optical phonon for the material i.

Following Li and Chen,[8] we obtain the eigenfrequencies for the heterostructures in the cylindrical dots. The matching boundary conditions are adjusted to take into consideration the presence of the barrier material in the heterostructure. For the TSO mode, we obtain $\epsilon_1(\omega)/\epsilon_2(\omega)=-\tanh(qd)$ and $\epsilon_1(\omega)/\epsilon_2(\omega)=-\coth(qd)$ for the symmetric and antisymmetric TSO mode, respectively. Using Eq. (1), two biquadratic equations appear for the symmetric and antisymmetric TSO modes [Eqs. (A1) and (A2) in the Appendix].

For the SSO mode, the boundary conditions applied to the lateral surface solution give rise to the eigenfrequency relation similar to Eq. (28) reported in Ref. 8. Inserting the di-

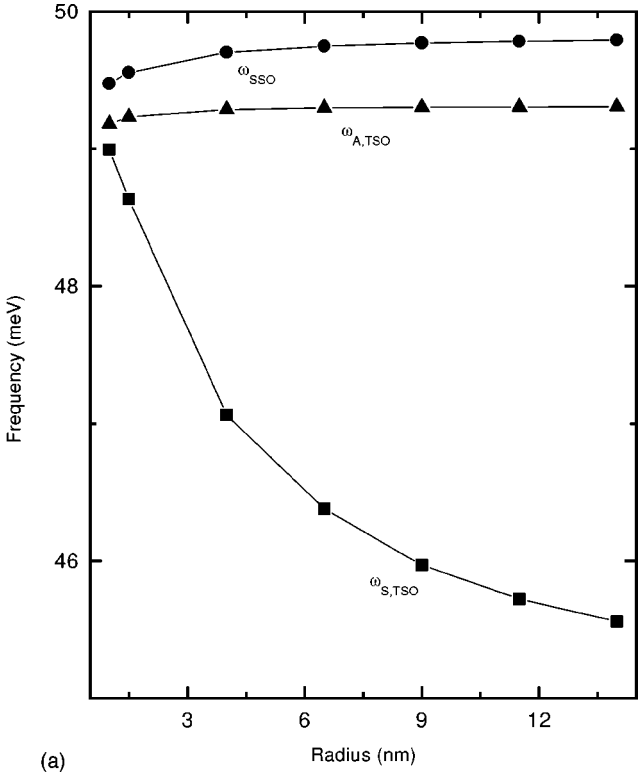

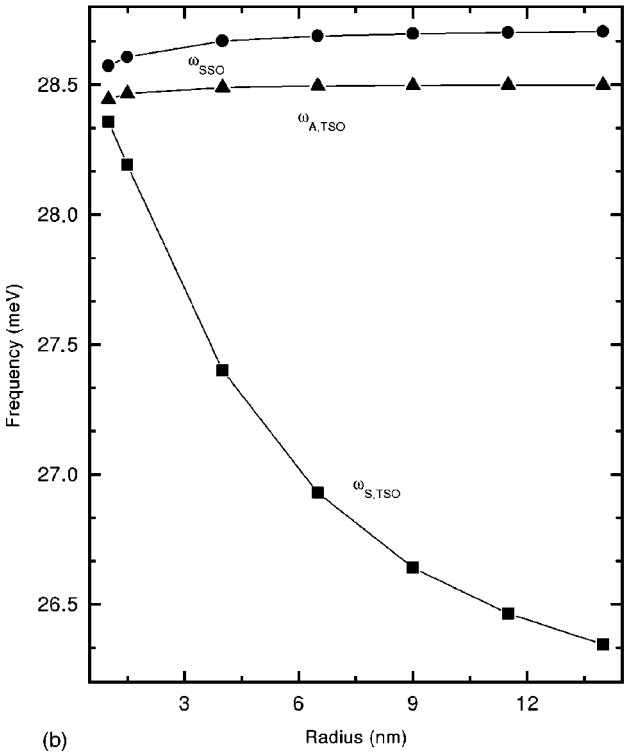

FIG. 1. (a) Frequencies of vibration for the surface-optical modes in a cylindrical AlAs free-standing quantum dot as a function of the cylinder radius. The lines are guides for the eyes. (b) Frequencies of vibration for the surface-optical modes in a cylindrical InAs free-standing quantum dot as a function of the cylinder radius. The lines are guides for eyes.

electric functions given by Eq. (1) into this eigenfrequency relation, a biquadratic equation for the SSO modes is found [Eq. (A3) in the Appendix]. All the Bessel functions appearing in the above relations are evaluated using the Fortran-Mathematical Library IMSL.[10]

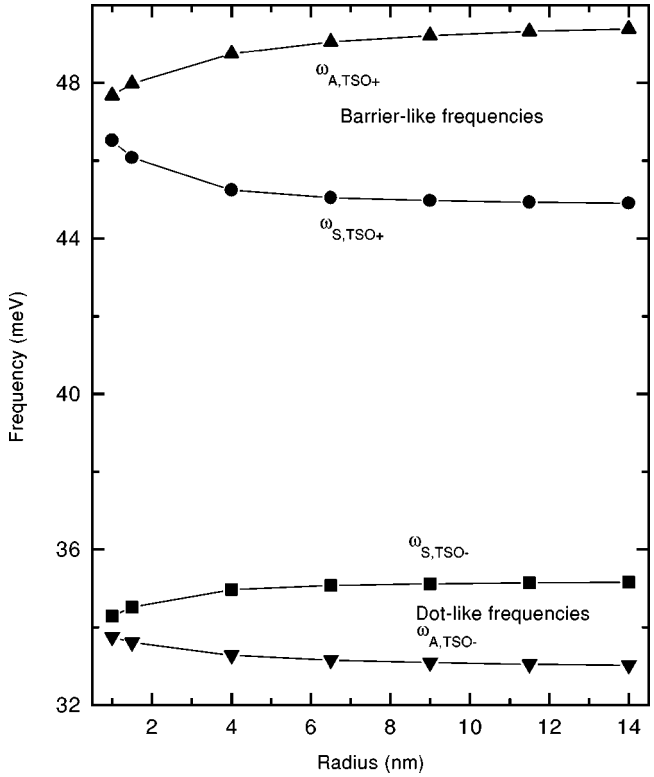

FIG. 2. Frequencies of symmetric and antisymmetric TSO modes in a GaAs/AlAs cylindrical quantum dot (with $d=0.8$ nm) as a function of the cylinder radius. The lines are guides for the eyes.

III. RESULTS AND DISCUSSION

In this section we present the optical-phonon eigenfrequencies for the free-standing dots and for the heterostructures ones. Since the LO phonon modes are independent of the geometrical parameters of the dot, we will focus our discussion on the IF modes. For all the surface (interface) phonons, the intersubband transitions are neglected. It is assumed that electrons occupy only the ground subband,[7,11] in the ''extreme quantum limit.'' Therefore, only the lowest-surface phonon modes ($m=0$) are discussed.

We consider quantum dots having 6 ML, i.e., ≈ 1.6 nm of the thickness. Similar values have been used in the literature[12] to calculate the ground-state energy for a quantum disk. The values of ϵ_0, ϵ_∞, ω_{LO}, and ω_{TO} used to evaluate phonon frequencies are taken from Ref. 14. Figure 1 shows the results for AlAs and InAs free-standing dots. A symmetric and an antisymmetric TSO mode is found. For both materials, we obtain a strong dependence of the symmetric mode $\omega_{S,TSO}$ with the dot radius. For $R<6$ nm, $\omega_{S,TSO}$ decreases strongly and tends to a bulk-limiting value for $R>10$ nm [see Figs. 1(a) and 1(b)]. On the contrary, the antisymmetric modes $\omega_{A,TSO}$ depend on the radius very weakly. For small values of R, $\omega_{A,TSO}$ increases very slowly and becomes constant for $R>8$ nm. It is observed that the SSO mode ω_{SSO} is higher than the frequencies $\omega_{S,TSO}$ and $\omega_{A,TSO}$; i.e., $\omega_{S,TSO}<\omega_{A,TSO}<\omega_{SSO}$ for $1\leqslant R\leqslant 14$ nm.

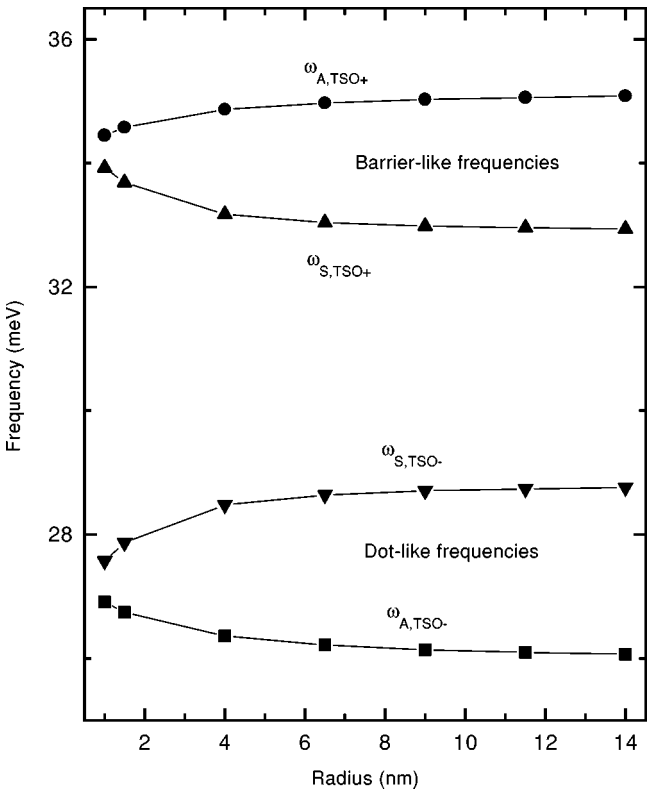

FIG. 3. Frequencies of symmetric and antisymmetric TSO modes in an InAs/GaAs cylindrical quantum dot (with $d=0.8$ nm) as a function of the cylinder radius. The lines are guides for the eyes.

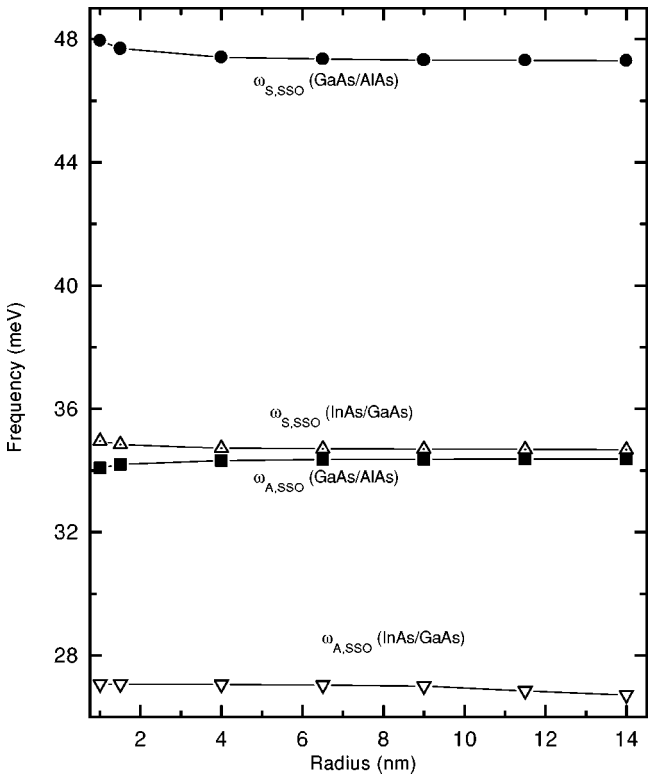

FIG. 4. Frequencies of vibration for the symmetric and antisymmetric SSO modes in cylindrical quantum dots GaAs/AlAs and InAs/GaAs (with $d=0.8$ nm) as a function of the cylinder radius. The lines are guides for the eyes.

Since the radius dependence of the SSO mode is practically negligible, a dimension-independent behavior for the frequency ω_{SSO} is expected. Similar results have been found in spherical quantum dots.[6]

Figures 2–4 depict the results for cylindrical GaAs/AlAs and InAs/GaAs quantum dots. Both the symmetric and antisymmetric TSO modes are weakly dependent of dot radius for $R \leqslant 5$ nm, as shown in Figs. 2 and 3. Each mode consists of two branches; $\omega_{S,TSO+}$ and $\omega_{S,TSO-}$ for the symmetric mode and $\omega_{A,TSO+}$ and $\omega_{A,TSO-}$ for the antisymmetric mode. The modes $\omega_{S,TSO+}$ and $\omega_{A,TSO+}$ have the barrierlike characteristics while the $\omega_{S,TSO-}$ and $\omega_{A,TSO-}$ ones are dot-type modes. The upper antisymmetric branch $\omega_{A,TSO+}$ increases with R and finally approaches the barrier bulklike frequency, while the lower branch $\omega_{A,TSO-}$ decreases to the dot bulklike frequency. For the symmetric mode, the opposite behavior is observed.

The surface-side frequencies are radius independent as shown in Fig. 4. As in the TSO modes, ω_{SSO+} have the barrierlike characteristics while the ω_{SSO-} are dot-type modes. This radius independence appears to be a consequence of the invariance of the electrostatic potential upon rotation around the z axis. Englman and Ruppin[15] have predicted a threefold-degenerate surface phonon modes with vibrations in the r, θ, and z directions of a cylinder. Therefore, the light incident parallel to the z axis of the cylinder excites only the z vibrations, whereas the light incident perpendicular to this axis excites both the r and θ phonons; thus showing stronger scattering intensity in the Raman experimental spectra.[16] Keeping the cylinder-height constant, one can expect that the SSO modes, which are obtained by imposing boundary conditions at $|z|=d$, to be practically less sensitive to the change in the r direction.

As expected, the plot of TSO frequencies as a function of the adimensional qR parameter shows that the symmetric and antisymmetric modes converge as $qR \rightarrow \infty$. This effect was also observed in GaAs/AlAs quantum wells and wires.[4] For the free-standing systems, the convergence values are shifted up to bulklike ω_{LO}, while the effect of the finite barriers in heterostructures tends to reduce these convergence values to $\approx(\omega_{TO}+\omega_{LO})/2$.

IV. CONCLUSION

Within the dielectric continuum framework, we have calculated the surface-mode frequencies in the cylindrical dots for both cases: free-standing in vacuum and heterostructure configuration. Both symmetric and antisymmetric modes diverge for great values of the cylinder radius. Surface-side optical modes are radius independent in the heterostructures while they present a slight dependence with the cylinder size in the free-standing case for $R<2$ nm. One can expect that the application of an electric field or any excitation in the z-growth direction will behave differently from that applied perpendicularly to that direction. We have restricted our calculations to the phonon-mode frequencies. These results will be used to evaluate electron-phonon scattering rates and optical phonon contribution to the ground-state energy of the system due to the deformation potential coupling.

ACKNOWLEDGMENTS

C.K.M. is indebted to A.E.C.I. (Agencia Española de Cooperación Internacional) for its financial support. The authors are grateful to Dr. Ramiro Pareja (Universidad Carlos III de Madrid, Spain) and Augusto Alcalde (Universidade Estadual de Campinas, Brazil) for their critical reading of the manuscript.

APPENDIX

The use of eigenfrequency relations and the Lyddane-Sachs-Teller expression gives rise to these two biquatric equations for the TSO modes:

$$(\epsilon_{+,\infty}-\epsilon_{-,\infty}e^{-2q_+d})\omega^4-\{(\epsilon_{+,\infty}-\epsilon_{-,\infty}e^{-2q_+d})\times(\omega_{1,TO}^2+\omega_{2,TO}^2)+\epsilon_1'(1+e^{-2q_+d})\omega_{1,TO}^2+\epsilon_2'(1-e^{-2q_+d})\omega_{2,TO}^2\}\omega^2+[(\epsilon_{+,\infty}-\epsilon_{-,\infty}e^{-2q_+d})+\epsilon_1'(1+e^{-2q_+d})+\epsilon_2'(1-e^{-2q_+d})]\omega_{1,TO}^2\omega_{2,TO}^2=0, \quad \text{(A1)}$$

and

$$(\epsilon_{+,\infty}+\epsilon_{-,\infty}e^{-2q_-d})\omega^4-\{(\epsilon_{+,\infty}+\epsilon_{-,\infty}e^{-2q_-d})\times(\omega_{1,TO}^2+\omega_{2,TO}^2)+\epsilon_1'(1+e^{-2q_-d})\omega_{1,TO}^2+\epsilon_2'(1-e^{-2q_-d})\omega_{2,TO}^2\}\omega^2+[(\epsilon_{+,\infty}+\epsilon_{-,\infty}e^{-2q_-d})+\epsilon_1'(1-e^{-2q_-d})-\epsilon_2'(1+e^{-2q_-d})]\omega_{1,TO}^2\omega_{2,TO}^2=0, \quad \text{(A2)}$$

where $\epsilon_{-,\infty}=\epsilon_{2,\infty}-\epsilon_{1,\infty}$ and $\epsilon_{+,\infty}=\epsilon_{1,\infty}+\epsilon_{2,\infty}$.

In both these expressions, $\epsilon_1'=\epsilon_{1,0}-\epsilon_{1,\infty}$ and $\epsilon_2'=\epsilon_{2,0}-\epsilon_{2,\infty}$. The vectors q_+ and q_- correspond to the roots of the transcendental [Eqs. (18) and (19)] given in Ref. 8.

For the SSO mode, by analogy and using the corresponding SSO-eigenfrequency relation, we obtain

$$[\epsilon_{1,\infty}K_0(\kappa R)I_1(\kappa R)+\epsilon_{2,\infty}I_0(\kappa R)K_1(\kappa R)]\omega^4-[K_0(\kappa R)I_1(\kappa R)(\omega_{2,TO}^2\epsilon_{1,\infty}+\epsilon_{1,0}\omega_{1,TO}^2)+I_0(\kappa R)K_1(\kappa R)(\omega_{2,TO}^2\epsilon_{2,0}+\epsilon_{2,\infty}\omega_{1,TO}^2)]\omega^2+\omega_{1,TO}^2\omega_{2,TO}^2[\epsilon_{1,0}K_0(\kappa R)I_1(\kappa R)+\epsilon_{2,0}I_0(\kappa R)K_1(\kappa R)]=0. \quad \text{(A3)}$$

Inside the dot, $\kappa=n\pi/2d$, n being an integer $(n\neq 0)$.

*Electronic address: clement@elrond.uc3m.es

†Electronic address: rmc@elrond.uc3m.es

[1] M. H. Degani and G. A. Farias, Phys. Rev. B **41**, 3572 (1990).

[2] J. M. Moison, F. Houzay, F. Barthe, L. Leprince, E. André, and O. Vatel, Appl. Phys. Lett. **64**, 196 (1994).

[3] L. Goldstein, F. Glas, J. Y. Marzin, M. N. Charasse, and G. Le Roux, Appl. Phys. Lett. **47**, 1099 (1985); J. M. Gerald, *ibid.* **61**, 2096 (1992).

[4] See, for example, K. W. Kim, M. A. Stroscio, A. Bhatt, R. Mickevicius, and V. V. Mitin, J. Appl. Phys. **70**, 319 (1991), and references therein.

[5] R. M. de la Cruz, Superlattices Microstruct. **16**, 427 (1994).

[6] R. M. de la Cruz, S. W. Teitsworth, and M. A. Stroscio, Phys. Rev. B **52**, 1489 (1995).

[7] N. C. Constantinou and B. K. Ridley, J. Phys.: Condens. Matter **1**, 2283 (1989).

[8] W.-S. Li and C.-Y. Chen, Physica B **229**, 375 (1997).

[9] M. C. Klein, F. Hache, D. Ricard, and C. Flytzanis, Phys. Rev. B **42**, 11 123 (1990); J. J. Licari and E. Evrard, *ibid.* **15**, 2254 (1977).

[10] ISML Math/Library: *Fortran Subroutines for Mathematical Applications* (Visual Numerics, Houston, 1994).

[11] X. F. Wang and X. L. Lei, Phys. Rev. B **49**, 4780 (1994).

[12] G. Lamouche and Y. Lépine, Phys. Rev. B **51**, 1950 (1995).

[13] J. Y. Marzin, and G. Bastard, Solid State Commun. **92**, 437 (1994).

[14] S. Adachi, *Properties of Aluminium Gallium Arsenide* (IEE, London, 1993); J. Appl. Phys. **58**, R1 (1985).

[15] R. Englman and R. Ruppin, J. Phys. C **1**, 614 (1968).

[16] M. Watt, H. E. G. Arnot, C. M. Sotomayor Torres, and S. P. Beaumont, in *Nanostructure Physics and Fabrication*, edited by Mark A. Reed and Wiley P. Kirk (Academic Press, New York, 1989), p. 89.